Extremum-Seeking Finite-Time Optimal Control of Plasma Current Profile at the DIII-D Tokamak

Y. Ou, C. Xu, E. Schuster, T. C. Luce, J. R. Ferron and M. L. Walker

***Abstract*— In a magnetic fusion reactor, the achievement of a certain type of plasma current profiles, which are compatible with magnetohydrodynamic (MHD) stability at high plasma pressure, is key to enable high fusion gain and noninductive sustainment of the plasma current for steady-state operation. The approach taken toward establishing such plasma current profiles at the DIII-D tokamak is to create the desired profile during the plasma current ramp-up and early flattop phases. The evolution in time of the current profile is related to the evolution of the poloidal flux, which is modeled in normalized cylindrical coordinates using a partial differential equation (PDE) usually referred to as the magnetic diffusion equation. The control problem is formulated as an open-loop, finite-time, optimal control problem for a nonlinear distributed parameter system, and is approached using extremum seeking. Simulation results, which demonstrate the accuracy of the considered model and the efficiency of the proposed controller, are presented.**

I. Introduction

In a fusion reaction, two light nuclei stick together to form a heavier nucleus. The total mass after the reaction is less than that before. The "lost" mass appears as energy, with the amount given by the famous Einstein formula $E = (M_r - M_p)c^2$, where E is the energy, M_r is the mass of the reactant nuclei, M_p is the mass of the product nuclei, and c is the speed of light. Since nuclei carry positive charges, they normally repel one another. To overcome the Coulomb barrier, the kinetic energy of the nuclei is increased by heating. The higher the temperature, the faster the atoms or nuclei move. The fuel must be heated to temperatures around 100 million degrees at which the nuclei overcome the force of repulsion of the positive charges when they collide, and fuse. At much lower temperatures (about 10 thousand degrees), the electrons and nuclei separate and create an ionized gas called plasma. In a plasma, the electrons are stripped from the nuclei of the atoms resulting in an ionized gas where positively and negatively charged particles move independently. Importantly, the particles in a plasma are charged, conduct electricity and interact with magnetic fields. Magnetic confinement fusion [1] exploits this property of the plasma and uses magnetic fields to exert a force on the hydrogen atoms which have been ionized. The tokamak [2] concept invented in the Soviet Union in the late 1950's is now the major and most promising magnetic confinement approach being pursued around the world. Tokamak is an acronym developed from the Russian words TOroidalnaya KAmera ee MAgnitnaya Katushka which means "toroidal chamber with magnetic coils". The tokamak uses field lines bent into a torus so that there is no end. In a tokamak, the toroidal magnetic field is produced by the so-called "toroidal field" (TF) coils. Addition of a poloidal field generated by the toroidal plasma current and the "poloidal field" (PF) coils, which is necessary for the existence of a magnetohydrodynamic (MHD) equilibrium [3], produces a combined field in which the magnetic field lines twist their way around the tokamak to form a helical structure. A more in-depth introduction to fusion can be found in [4], [5], [6], in which considerable effort was made to describe the current problems of tokamak plasma control at a level that is accessible to engineers, mathematicians, and non-plasma physicists.

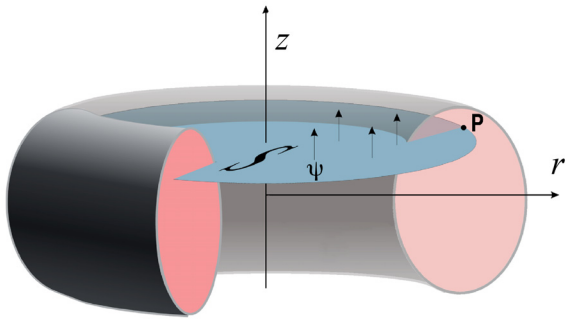

Fig. 1. Poloidal flux in a tokamak.

It is possible to use the poloidal component of the helicoidal magnetic lines to define nested toroidal surfaces corresponding to constant values of the poloidal magnetic flux. As it is illustrated in Fig. 1, the poloidal flux ψ at a point P in the (r,z) cross section of the plasma (i.e., poloidal cross section) is the total flux through the surface S bounded by the toroidal ring passing through P, i.e., $\psi = \frac{1}{2\pi}\int B_{pol} dS$. Thus, the poloidal flux ψ can be used as a spatial coordinate.

The need to optimize the tokamak concept for the design of an economical, possibly steady-state, fusion power plant have motivated extensive international research aimed at finding the so-called advanced tokamak (AT) operation scenarios [7]. Such regimes are characterized by a high confinement state with improved MHD stability, which yields a strong improvement of the plasma performance quantified

This work was supported in part by a grant from the Commonwealth of Pennsylvania, Department of Community and Economic Development, through the Pennsylvania Infrastructure Technology Alliance (PITA), the NSF CAREER award program (ECCS-0645086), and General Atomics (DoE contract number DE-FC02-04ER54698).

Y. Ou (yoo205@lehigh.edu), C. Xu and E. Schuster are with the Department of Mechanical Engineering and Mechanics, Lehigh University, Bethlehem, PA 18015, USA

T. C. Luce, J. R. Ferron and M.L. Walker are with General Atomics, San Diego, California, USA

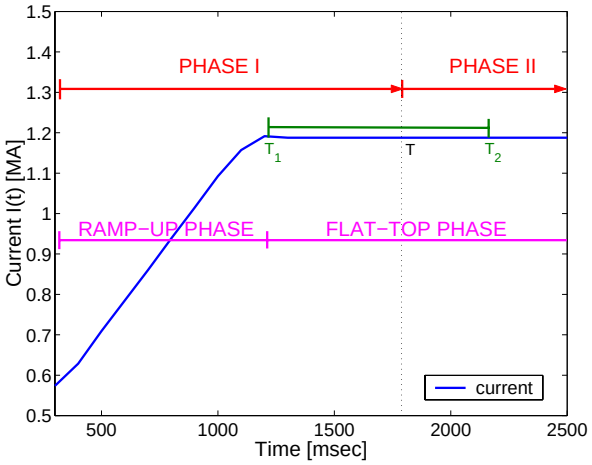

Fig. 2. Current Evolution.

by the increase of the energy confinement time and plasma pressure. In such conditions a dominant fraction of the plasma current is self-generated and the requirement on externally driven non-inductive current (a method of driving plasma current in a tokamak that does not depend on transformer action (e.g., by using RF waves or neutral beams); necessary for a continuously operated power plant, since the inductive current based on transformer action is cyclic) for steady-state operation is reduced. Setting up a suitable current profile, characterized by a weakly reversed magnetic shear [7], has been demonstrated to be a key condition for one possible advanced scenario with improved confinement and possible steady-state operation [8].

Although this research area is in its infancy, recent experiments at different devices around the world (JET, DIII-D, JT-60U, Tore Supra) have demonstrated significant progress in achieving profile control. At JET (UK), different current and temperature equilibrium target profiles have been reached and sustained for several seconds during the flattop current phase [9], [10]. In contrast to the JET approach, experiments at DIII-D (US) focus on creating the desired current profile during the plasma current ramp-up and early flattop phases with the aim of maintaining this target profile during the subsequent phases of the discharge. Since the actuators that are used to achieve the desired target profile are constrained by physical limitations, experiments have shown that some of the desirable target profiles may not be achieved for all arbitrary initial condition. Therefore, a perfect matching of the desirable target profile may not be physically possible. In practice, the objective is to achieve the best possible approximate matching in a short time windows $[T_1, T_2]$ during the early flattop phase of the total plasma current pulse, as shown in Fig. 2. Thus, such a matching problem can be treated as an optimal control problem for a nonlinear PDE system.

Extremum seeking [11] is employed in this work to tackle a finite-time optimal control problem for a nonlinear, distributed-parameter system. Extremum seeking is applicable to systems where the input-to-output map, possible non-linear, is unknown but has an extremum. The objective of the extremum seeking algorithm is to find the set of input parameters that achieve the extremum. In this work, we use extremum seeking to obtain the evolutions of the control inputs in the time interval $[0, T]$ that minimize the quadratic error between the actual current profile at time $T \in [T_1, T_2]$ and a desired target profile. This work is aimed at saving long trial-and-error periods of time currently spent by fusion experimentalists trying to manually adjust the time evolutions of the actuators to achieve the desired current profile at sometime $T \in [T_1, T_2]$ during the early stage of the flattop phase. Simulation results show the effectiveness of this approach.

This paper is organized as follows. In Section II, a dynamic model for the poloidal flux ψ is introduced. Section III describes the control objectives during the different phases of the discharge. An open-loop control approach based on extremum seeking is introduced in Section IV. A simulation study showing the response of the proposed dynamic model and the effectiveness of the extremum seeking optimal control method is presented in Section V. Finally, conclusions and identified future work are presented in Section VI.

II. CURRENT PROFILE EVOLUTION MODEL

We let ρ be an arbitrary coordinate indexing the magnetic surface ($\psi =$ constant). Any quantity constant on each magnetic surface could be chosen as the variable ρ. We choose the mean geometric radius of the magnetic surface as the variable ρ, i.e., $\pi B_{\phi,o}\rho^2 = \Phi$, where Φ is the toroidal magnetic flux. The evolution of the poloidal flux in normalized cylindrical coordinates is given by the magnetic diffusion equation [12],

$$\frac{\partial \psi}{\partial t} = \frac{\eta(T_e)}{\mu_o \rho_b^2 \hat{F}^2 \hat{\rho}} \frac{\partial}{\partial \hat{\rho}} \left(\hat{\rho} \hat{F} \hat{G} \hat{H} \frac{\partial \psi}{\partial \hat{\rho}} \right) - R_o \hat{H} \eta(T_e) \frac{<\bar{j}_{NI} \cdot \bar{B}>}{B_{\phi,o}}, \quad (1)$$

where all the parameters are defined in Table I.

The model (1) is based on the following assumptions:

- The vacuum toroidal field is constant in time (usually true in practice).

TABLE I

A DESCRIPTION OF THE PARAMETERS

Parameters	Description
ψ	poloidal flux
$\eta(T_e)$	plasma resistivity
T_e	electron temperature
n	plasma density
$\mu_o = 4\pi \times 10^{-7}$ ($\frac{\mathrm{H}}{\mathrm{m}}$)	vacuum magnetic permeability
$\rho_b = 0.79$ (m)	radius of last closed flux surface
Φ_b	toroidal flux in the last closed flux surface
$B_{\phi,o} = 1.85\ T$	reference magnetic field at R_o
$R_o = 1.668$ (m)	reference point for $B_{\phi,o}$ (e.g., geometric center of plasma R_{geo})
$\hat{\rho}$	normalized radius $\frac{\rho}{\rho_b}$
$\hat{F}, \hat{G}, \hat{H}$	geometric factors (functions of $\hat{\rho}$ (Fig. 3))
$\bar{j}_{NI}$	any non-inductive source of current density (neutral beam, electron cyclotron, etc.)
$<>$	flux-surface average
j	plasma current density
I	total plasma current
P_{tot}	total power of non-inductive current drives
$\bar{n}$	spatially average density

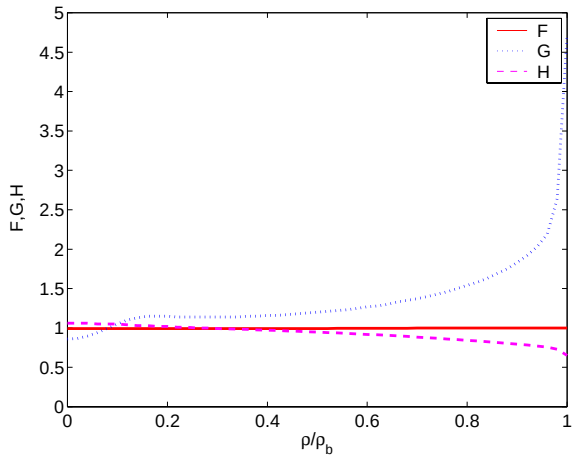

Fig. 3. Geometric factors F, G, and H.

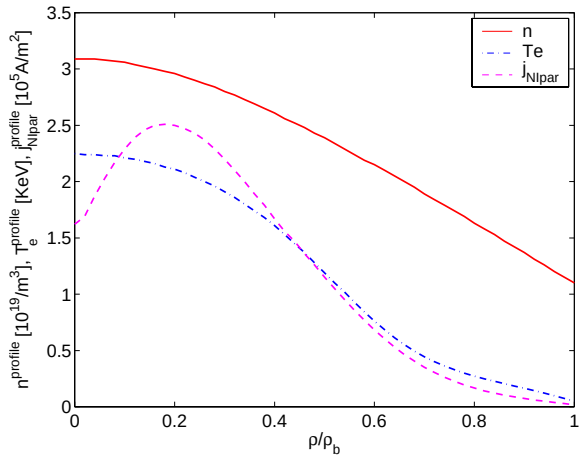

Fig. 4. Density ($n^{profile}$), temperature ($T_e^{profile}$), and non-inductive toroidal current density ($j_{NIpar}^{profile}(\hat{\rho})$) profiles.

- The map of $\hat{\rho}$ in real space is constant in time (approximately true if plasma boundary control regulates to a constant reference).

The boundary conditions of (1) are given by

$$\begin{aligned} \left.\frac{\partial \psi}{\partial \hat{\rho}}\right|_{\hat{\rho}=0} &= 0 \\ \left.\frac{\partial \psi}{\partial \hat{\rho}}\right|_{\hat{\rho}=1} &= \frac{\mu_o}{2\pi}\frac{R_o}{\hat{G}\big|_{\hat{\rho}=1}\hat{H}\big|_{\hat{\rho}=1}} I(t), \end{aligned} \tag{2}$$

where $I(t)$ denotes the total plasma current.

The current density that flows toroidally around the tokamak, $<\bar{j}\cdot\bar{B}/B_{\phi,o}>$, and whose profile must be controlled, is related to spatial derivative of the poloidal magnetic flux,

$$\frac{<\bar{j}\cdot\bar{B}>}{B_{\phi,o}} = \frac{1}{\mu_o \rho_b^2 \hat{F}^2 \hat{H}\hat{\rho}}\frac{\partial}{\partial\hat{\rho}}\left(\hat{\rho}\hat{F}\hat{G}\hat{H}\frac{1}{R_0}\frac{\partial\psi}{\partial\hat{\rho}}\right). \tag{3}$$

During "Phase I" (see Fig. 2), mainly governed by the ramp-up phase, the plasma current is mostly driven by induction. In this case, it is possible to decouple the equation for the evolution of the poloidal flux from the evolution equations for the temperature $T_e(\hat{\rho},t)$ and the density $n_e(\hat{\rho},t)$. Highly simplified models for the density, temperature, and non-inductive toroidal current density are chosen for this phase. The profile shapes are assumed to remain fixed. The responses to the actuators are simply scalar multiples of the reference profiles. These reference profiles are taken from a DIII-D tokamak discharge.

The density n is independently controlled, and can be written as

$$n(\hat{\rho},t) = n^{profile}(\hat{\rho})u_n(t), \tag{4}$$

where $n^{profile}$ is given in Fig. 4. The average density is defined as $\bar{n}(t) = \int_0^1 n(\hat{\rho},t)d\hat{\rho}$.

The temperature T_e is proportional to $\frac{I(t)\sqrt{P_{tot}}}{\bar{n}(t)}$, and can be written as

$$T_e(\hat{\rho},t) = k_{Te}T_e^{profile}(\hat{\rho})\frac{I(t)\sqrt{P_{tot}}}{\bar{n}(t)} \tag{5}$$

where $T_e^{profile}$ is given in Fig. 4, $k_{Te} = 1.7295\cdot 10^{10}$, and P_{tot} is the total power of the non-inductive current sources (Electron Cyclotron Heating (ECH), Neutral Beam Heating (NBH), etc.).

The non-inductive toroidal current density $\frac{<\bar{j}_{NI}\cdot\bar{B}>}{B_{\phi,o}}$ is written as

$$\frac{<\bar{j}_{NI}\cdot\bar{B}>}{B_{\phi,o}} = k_{NIpar}\, j_{NIpar}^{profile}(\hat{\rho})\frac{I(t)^{1/2}P_{tot}(t)^{5/4}}{\bar{n}(t)^{3/2}} \tag{6}$$

where $j_{NIpar}^{profile}$ is given in Fig. 4, and $k_{NIpar} = 1.2139\cdot 10^{18}$.

The resistivity η scales with the temperature T_e as

$$\eta(\hat{\rho},t) = \frac{k_{eff}Z_{eff}}{T_e^{3/2}(\hat{\rho},t)}, \tag{7}$$

where $Z_{eff} = 1.5$, and $k_{eff} = 4.2702\cdot 10^{-8}$.

We consider $\bar{n}(t)$, $I(t)$, and $P_{tot}(t)$ the physical actuators of the system.

III. CONTROL PROBLEM DESCRIPTION

The control objective, as well as the dynamic models for current profile evolution, depend on the phases of the discharge (Fig. 2). During "Phase I" the control goal is to drive the current profile from any arbitrary initial condition to a prescribed target profile at some time $T \in (T_1, T_2)$ (here $T_1 = 1.2s$ and $T_2 = 2.4s$) in the flat-top phase of the total current $I(t)$ evolution. However, since the available actuators during "Phase I" differ from those used during "Phase II" and are constrained by physical limitations, the prescribed target profile is not an equilibrium profile during "Phase I". During "Phase II" the control goal is to regulate the current profile using as little control effort as possible because the actuators are not only limited in power but also in energy. For this reason, the goal during "Phase I" is to set up an initial profile for "Phase II" as close as possible to its desirable profile.

In this paper, we focus on "Phase I." An optimal control problem must be solved, where control laws $I(t)$, $P_{tot}(t)$, and $\bar{n}(t)$ are sought to minimize the cost functional

$$J = \sqrt{\frac{1}{M}\min(J^*(t_j))}, \tag{8}$$

where t_j are discrete points in time equally spaced within the interval $[T_1, T_2]$, e.g., $t(j) = 1.2s, 1.3s, 1.4s, \ldots, 2.4s$ for $j = 1, 2, 3, \ldots, 13$, and $J^*(t_j)$ is given by

$$J^*(t_j) = \sum_{i=0}^{M} (\iota(\hat{\rho}_i, t_j) - \iota^{des}(\hat{\rho}_i))^2, \tag{9}$$

where M is the number of discrete points in space within the interval $[0,1]$ for the normalized radius.

For convenience, since experimentalists usually describe the target profile in terms of the inverse of the safety factor q, defined here as ι, the cost function (8) has been expressed in terms of this variable. The safety factor q and the figure of merit ι are related and defined as

$$\iota(\rho, t) = \frac{1}{q(\rho, t)} = 2\pi \frac{\partial \psi(\rho, t)}{\partial \Phi}. \tag{10}$$

The constant relationship between Φ and ρ, $\rho = \sqrt{\frac{\Phi}{\pi B_{\phi,o}}}$, and the definition of the normalized radius (in Table I) allow us to rewrite (10) as

$$\iota(\hat{\rho}, t) = \frac{\partial \psi}{\partial \hat{\rho}} \frac{1}{B_{\phi,o} \rho_b^2 \hat{\rho}}, \tag{11}$$

where $B_{\phi,o}$ and ρ_b are defined in Table I.

"Phase I" can be roughly divided into two phases, the ramp-up phase and the flattop phase. During the ramp-up phase, the three actuators $I(t)$, $\overline{n}(t)$ and $P_{tot}(t)$ are available, whereas during the flattop phase we can only vary $P_{tot}(t)$ keeping $I(t)$ and $\overline{n}(t)$ fixed at some predetermined values. In addition to this specific constraints during the flattop phase, the absolute values, and sometimes the derivatives in time, of the control variables must be within some specific limits during the whole "Phase I". The physical ranges for $I(t)$, $\overline{n}(t)$ and $P_{tot}(t)$ are given by

$$0 \le I(t) \le I_{max}, \quad \left| \frac{dI(t)}{dt} \right| \le dI_{max} \tag{12}$$

$$I(\mathrm{MA}) \le \frac{\overline{n}(t)}{10^{19}} \le 5I(\mathrm{MA}) \tag{13}$$

$$0 \le P_{tot}(t) \le P_{max}. \tag{14}$$

To accurately reproduce experimental discharges, we must add constraints for $I(t)$ and $\overline{n}(t)$ at the initial time of "Phase I", i.e.,

$$I(t = 0s) = I_0, \quad \overline{n}(t = 0s) = \overline{n}_0. \tag{15}$$

In addition, a value of the total current $I(t)$ is prescribed for the flattop phase, i.e.,

$$I(t \ge T_1) = I_{target}, \tag{16}$$

where T_1 marks the end of the ramp-up phase and the start of the flattop phase (Fig. 2).

In summary, the optimal control problem (8) must be solved taking into account that (i) during the ramp-up phase ($0 \le t \le T_1$) we can manipulate the three actuators by obeying the physical constraints (12)–(15), (ii) during flattop phase $I(t)$ is constrained by (16), and $\overline{n}(t)$ must be equal to $\overline{n}(T_1)$.

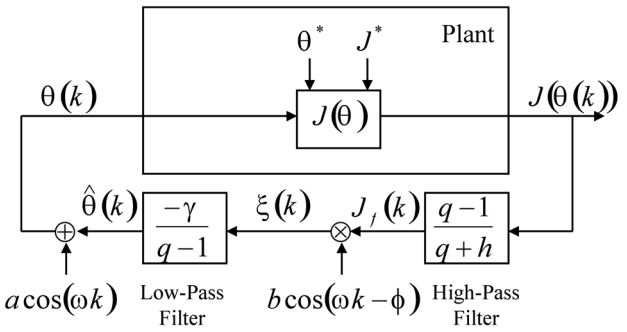

Fig. 5. Extremum seeking control scheme.

We seek $I(t)$, $\overline{n}(t)$ and $P_{tot}(t)$ for $t \in [0, T]$ that makes $\iota(\hat{\rho}, T)$ as close as possible to the prescribed target profile $\iota^{des}(\hat{\rho})$ at some time $T \in [T_1, T_2]$.

IV. EXTREMUM SEEKING OPTIMAL CONTROL

Extremum seeking control, a popular tool in control applications in the 1940-50's, has seen a resurgence in popularity as a real time optimization tool in different fields of engineering [11]. Extremum seeking is applicable in situations where there is a nonlinearity in the control problem, and the nonlinearity has a local minimum or a maximum. The parameter space can be multidimensional. Here, we use extremum seeking for iterative optimization of the structure parameters θ (shown in Fig. 5) to make the quadratic error between $\iota(\hat{\rho}, T)$ and the prescribed target profile $\iota^{des}(\hat{\rho})$ as small as possible at some time $T \in [T_1, T_2]$, i.e., to minimize J in (8).

We change the structure parameters θ after each simulated plasma "discharge." Thus, we employ the discrete time variant of extremum seeking [13]. The implementation is depicted in Figure 5, where q denotes the variable of the Z-transform. The high-pass filter is designed as $0 < h < 1$, and the modulation frequency ω is selected such that $\omega = \alpha\pi$, $0 < |\alpha| < 1$, and α is rational. The static nonlinear block $J(\theta)$ corresponds to one "discharge" of the system. The objective is to minimize J. If J has a global minimum, its value is denoted by J^* and its argument by θ^*. Given the simulated profile $\iota(\hat{\rho}, t)$, the output of the nonlinear static map, $J(k) = J(\theta(k))$, is obtained by evaluating (8) and used to compute $\theta(k+1)$ according to the extremum seeking procedure in the Figure 5, or written equivalently as

$$\begin{aligned} J_f(k) &= -hJ_f(k-1) + J(k) - J(k-1) && (17)\\ \xi(k) &= J_f(k) b \cos(\omega k - \phi) && (18)\\ \hat{\theta}(k+1) &= \hat{\theta}(k) - \gamma \xi(k) && (19)\\ \theta(k+1) &= \hat{\theta}(k+1) + a\cos(\omega(k+1)). && (20) \end{aligned}$$

We are dealing with a multi-parameter extremum seeking procedure (10 parameters). Thus, we write

$$\theta(k) = \begin{bmatrix} \theta_1(k) \\ \theta_2(k) \\ \vdots \\ \theta_{10}(k) \end{bmatrix}, \hat{\theta}(k) = \begin{bmatrix} \hat{\theta}_1(k) \\ \hat{\theta}_2(k) \\ \vdots \\ \hat{\theta}_{10}(k) \end{bmatrix}, \xi(k) = \begin{bmatrix} \xi_1(k) \\ \xi_2(k) \\ \vdots \\ \xi_{10}(k) \end{bmatrix}.$$

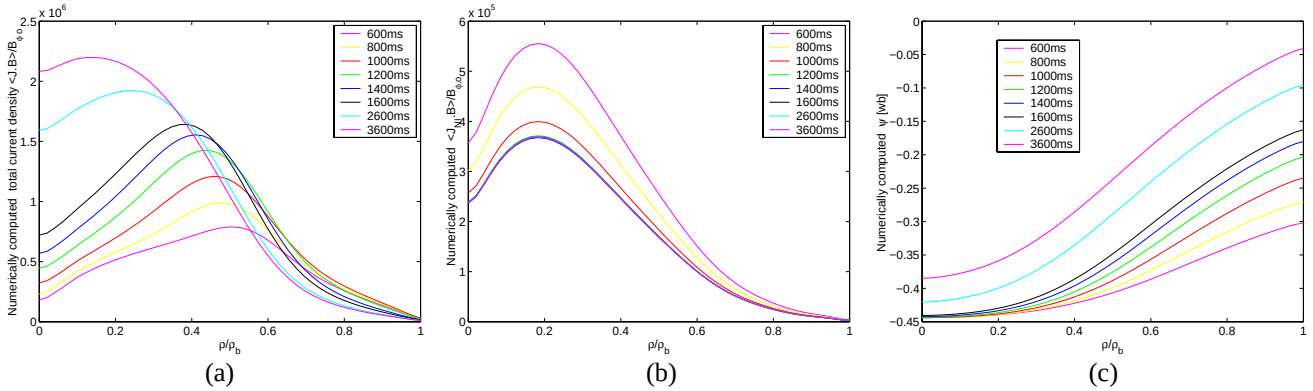

Fig. 6. Profile evolutions in a simulated "discharge": (a) $\frac{<\bar{j}\cdot\bar{B}>}{B_{\phi,o}}$, (b) $\frac{<\bar{j}_{NI}\cdot\bar{B}>}{B_{\phi,o}}$, (c) ψ.

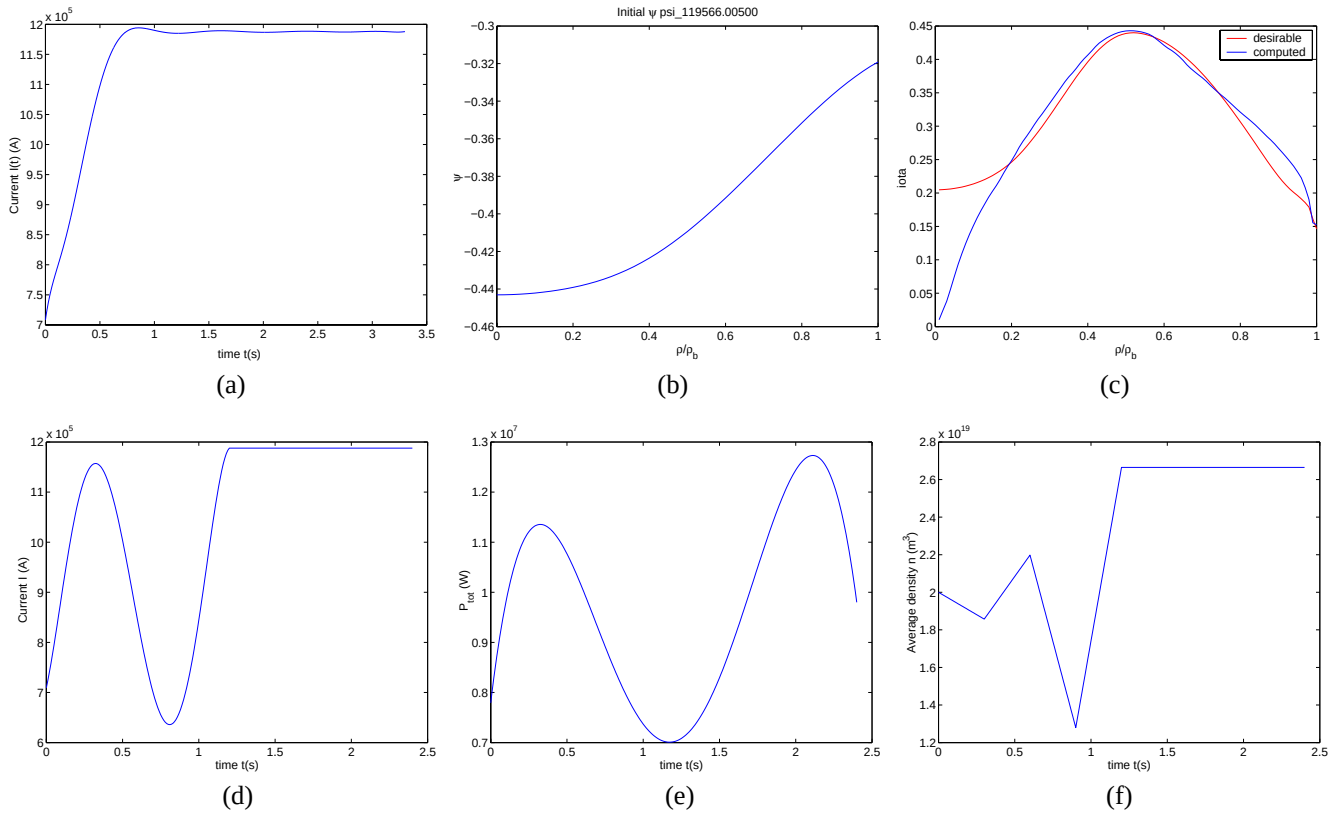

Fig. 7. Simulation of extremum seeking optimal control: (a) Current $I(t)$ evolution ,(b) initial ψ profile extracted from experimental shot 119566, (c) Desired target profile and computed best matching, (d) $I(t)$, (e) P_{tot}, (f) $\bar{n}(t)$.

The extremum seeking constants shown in Figure 5 are written as

$$\begin{aligned} a &= b = diag\left([a_1 \quad a_2 \quad \cdots \quad a_{10}]\right) \\ \gamma &= diag\left([\gamma_1 \quad \gamma_2 \quad \cdots \quad \gamma_{10}]\right). \end{aligned}$$

In addition, we denote

$$\cos(\omega k) = \begin{bmatrix} \cos(\omega_1 k) \\ \cos(\omega_2 k) \\ \vdots \\ \cos(\omega_{10} k) \end{bmatrix}, \cos(\omega k - \phi) = \begin{bmatrix} \cos(\omega_1 k - \phi_1) \\ \cos(\omega_2 k - \phi_2) \\ \vdots \\ \cos(\omega_{10} k - \phi_{10}) \end{bmatrix}.$$

In a simulation environment, we understand by "discharge" the integration of the PDE equation (1)–(2). In each iteration of the extremum seeking procedure, $\theta(k)$ is used to compute the time evolution of the three physical actuators $I(t)$, $\bar{n}(t)$ and $P_{tot}(t)$. The vector parameter θ has 10 components,

$$\begin{aligned} \theta = [&I(0.4s), I(0.8s), P_{tot}(0s), P_{tot}(0.4s), P_{tot}(0.8s), \\ &P_{tot}(1.2s), \bar{n}(0.3s), \bar{n}(0.6s), \bar{n}(0.9s), \bar{n}(1.2s)] \end{aligned} \quad (21)$$

By taking into account that $I(0s) = I_0$ and $I(T_1) = I_{target}$, and using polynomial curve fitting for the points $I(0s), I(0.4s), I(0.8s), I(1.2s)$, we can reconstruct the profile for $I(t)$ for $t \in [0, T_1]$. In addition, we make $I(t) = I_{target}$ for $t \in (T_1, T_2]$. Following similar procedure, we can reconstruct the law for $P_{tot}(t)$. By considering that $\bar{n}(0s) = \bar{n}_0$, and using linear interpolation, we can define the law for $\bar{n}(t)$. The reconstructed control laws are in turn fed into the PDE

system (1)–(2). Given ψ_{ini}, the PDE equation is integrated to obtain $\psi(\hat{\rho},t)$, and finally $\iota(\hat{\rho},t)$, which are necessary to evaluate the cost function, $J(k) = J(\theta(k))$, in (8).

V. SIMULATION RESULTS

In this section, we present simulation results showing both the dynamic response of the model proposed for the inductive "Phase I" and the effectiveness of the extremum seeking design to solve the optimal control problem (8).

A. Dynamic Response of Inductive-Phase Model

In this simulation, we consider the time interval $[0.5s, 3.6s]$. The current $I(t)$ evolution is shown in Fig. 7-(a), whereas the initial poloidal flux ψ is shown in Fig. 7-(b). The average density scales with the current, i.e., $n(t)(10^{19}m^{-3}) = 3I(t)$ (MA), and the total power $P_{tot}(t)$ is kept constant at 5.0(MW).

The system of equations describing the poloidal flux evolution has been successfully implemented in a numerical solver. Fig. 6 shows the profile evolutions for the total current density $\frac{<j\cdot B>}{B_{\phi,o}}$, the non-inductive current density $\frac{<j_{NI}\cdot B>}{B_{\phi,o}}$, and the poloidal flux ψ, based on the dynamic model (1)–(7). As expected, the area under the current density curve increases with time, consistent with the boundary condition related to the total current at $\hat{\rho} = 1$ and the current $I(t)$ evolution shown in Fig. 7-(a). The maximum of the current density moves slowly towards an smaller radius, as expected from a diffusive process. Given the three order of magnitude variation in the plasma resistivity (small in the hot center and large at the cold edge), the current density rapidly equilibrates at the edge, but evolves much more slowly in the center. The small spatial scale structure in ι and q at a small radius is an artifact of the numerical scheme used to derive these variables from the calculated poloidal flux. The simulated profile evolutions show qualitative agreement with tokamak experiments.

B. Optimal Control via Extremum Seeking

In this case we consider the time interval $[0, T_2 = 2.4s]$. The current $I(t)$ is reconstructed in $[0, T_1]$ using polynomial interpolation to fit the discrete points $I(t=0) = 0.709229$ MA, $I(t=0.4s) = \theta_1$, $I(t=0.8s) = \theta_2$, $I(t = T_1 = 1.2s) = 1.18774$ MA. In addition, $I(t) = 1.18774$ MA in $(T_1, T_2]$. The parameters $I_{max} = 1.19141$ MA and $dI_{max} = 2$ MA/s are used in (12) to evaluate the constraints for $I(t)$.

The total power $P_{tot}(t)$ is reconstructed using polynomial interpolation to fit the discrete points $P_{tot}(t=0) = \theta_3$, $P_{tot}(t = 0.4s) = \theta_4$, $P_{tot}(t=0.8s) = \theta_5$, $P_{tot}(t = T_1 = 1.2s) = \theta_6$. For $t > T_1 = 1.2s$, $P_{tot}(t) = P_{tot}(T_1)$. The constraint for $P_{tot}(t)$ is evaluated from (14) using $P_{max} = 20$ MW.

The average density $\bar{n}(t)$ is obtained by similar procedure, given the discrete points $\bar{n}(t=0) = 2\times 10^{10}m^{-3}$, $\bar{n}(t = 0.3s) = \theta_7$, $\bar{n}(t=0.6s) = \theta_8$, $\bar{n}(t=0.9s) = \theta_9$, $\bar{n}(t = T_1 = 1.2s) = \theta_{10}$. For $t > T_1 = 1.2s$, $\bar{n}(t) = \bar{n}(T_1)$. The constraints for $\bar{n}(t)$ are given by (13).

The initial values for θ are arbitrarily chosen as follows

$$\begin{aligned}\theta_{int} \;=\; & [0.938721\,MA, 1.15723\,MA, 1.15723\,MW,\\ & 0.860596\,MW, 1.09253\,MW, 1.09253\times 2\,MW,\\ & 1\times 10^{19}m^{-3}, 2\times 10^{19}m^{-3}, 4\times 10^{19}m^{-3}].\end{aligned}$$

The initial poloidal flux ψ is shown in Fig. 7-(b). The target ι profile is shown in Fig. 7-(c).

A minimum is reached in less than 300 iterations of the extremum seeking algorithm. The corresponding time evolutions for the three actuators are shown in Fig. 7-(d), Fig. 7-(e), and Fig. 7-(f).

VI. CONCLUSIONS AND FUTURE WORKS

A simplified dynamic model describing the evolution of the poloidal flux, and therefore the ι profile, during the inductive phase of the discharge has been introduced. Simulation results show qualitative agreement with experiments.

A multi-parameter, extremum-seeking, open-loop, optimal controller has been designed, and successfully tested in simulations, to match a desired ι profile within a predefined time window during the flattop phase of the tokamak discharge. The extremum-seeking procedure has shown to be effective to deal with an optimal control problem defined for a nonlinear PDE system subject to many constraints in its actuators. Based on the promising results obtained in the simulation study, it is anticipated that the scheme can play an important role in fusion plasma physics experiments at the DIII-D tokamak.

REFERENCES

[1] J. Sheffield, "The physics of magnetic fusion reactors," *Reviews of Modern Physics*, vol. 66, no. 3, pp. 1015–1103, 1994.

[2] J. Wesson, *Tokamaks*, 3rd ed. Clarendon Press, Oxford, 2004.

[3] J. P. Freidberg, *Ideal magnetohydrodynamics*. New York: Plenum Press, 1987.

[4] A. Pironti and M. Walker, "Control of Tokamak Plasmas," *IEEE Control System Magazine*, vol. 25, no. 5, pp. 24–29, 2005.

[5] ——, "Fusion, tokamaks, and plasma control," *IEEE Control System Magazine*, vol. 25, no. 5, pp. 30–43, 2005.

[6] E. Schuster and M. Ariola, "The Role of Controls in Nuclear Fusion," in *Proceedings of the 45th IEEE Conference on Decision and Control*, 2006.

[7] T. Taylor *et al.*, "Physics of advanced tokamaks," *Plasma Physics and Controlled Fusion*, vol. 39, no. suppl. 12B, pp. B47–B73, 1997.

[8] M. Murakami *et al.*, "Progress toward fully noninductive, high beta conditions in DIII-D," *Physics of Plasmas*, vol. 13, no. 5, pp. 056–106, 2006.

[9] D. Moreau *et al.*, "Real-time control of the q-profile in JET for steady state advanced tokamak operation," *Nuclear Fusion*, vol. 43, no. 9, pp. 870–82, 2003.

[10] L. Laborde *et al.*, "Towards fully non-inductive current drive operation in JET," *Plasma Physics and Controlled Fusion*, vol. 47, no. 1, pp. 155–83, 2005.

[11] K. Ariyur and M. Krstic, *Real-Time Optimization by Extremum Seeking Feedback*. Wiley, 2003.

[12] F. Hinton and R. Hazeltine, "Theory of plasma transport in toroidal confinement systems," *Reviews of Modern Physics*, vol. 48, no. 2, pp. 239–308, 1976.

[13] K. A. J. Choi, M. Kristic and J. Lee, "Extremum seeking control for discrete-time systems," *IEEE Transactions on Automatic Control*, vol. 47, no. 2, pp. 318–323, 2002.